Materials Characterization 196 (2023) 112583

Contents lists available at ScienceDirect

Materials Characterization

journal homepage: www.elsevier.com/locate/matchar

In-situ TEM investigation of deformation mechanisms of twinning-induced plasticity steel

Jin-Kyung Kim

Department of Materials Science and Chemical Engineering, Hanyang University, Ansan 15588, Republic of Korea

ARTICLE INFO

Keywords:
In-situ TEM mechanical testing
Transmission electron microscopy (TEM)
Deformation mechanisms
TWIP steel
Deformation twin

ABSTRACT

High Mn twinning-induced plasticity (TWIP) steels have been the focus of research in the past decade due to their superior combination of strength and ductility. In-situ TEM mechanical testing is an efficient tool to provide direct insights into fundamental deformation mechanisms of materials, and thus, key observations by in-situ TEM mechanical testing are required to unravel the deformation mechanisms of TWIP steels. The present work reports three deformation mechanisms of TWIP steels observed by in-situ TEM mechanical testing: (1) formation of deformation twins from grain boundaries, (2) interference of growth of a deformation twin by a stacking fault, and (3) motion of extended dislocations contributing to the plasticity. Firstly, the formation of deformation twins by direct emission of Shockley partial dislocations from grain boundary sources was observed. The different degree of the motion of twinning partial dislocations indicates a different degree of growth kinetics of deformation twins depending upon local stress states. Secondly, Shockley partial dislocations moved in an inclined twin confined between a precipitate and a stacking fault, thereby leading to the growth of the deformation twin. The sluggish motion of Shockley partial dislocations near the stacking fault indicates a strengthening effect of stacking faults. Thirdly, direct evidence of motion of extended dislocation across the entire grain was obtained, which suggests a contribution of extended dislocation slip on the plasticity of TWIP steels.

1. Introduction

High Mn twinning-induced plasticity (TWIP) steels have been the focus of research in the past decade due to their superior combination of strength and ductility [1]. The superior mechanical properties mainly originate from dynamic interactions between deformation twins (DT) and dislocations upon deformation [2]. During deformation of TWIP steels, slip occurs at the initial stage of deformation and combined slip and deformation twinning occurs after reaching the critical strain of deformation twinning [2]. The stacking fault energy (SFE) plays a key role in determining plasticity enhancing mechanisms of TWIP steels such as deformation twinning or deformation-induced martensitic transformation. While the low SFE favors the deformation-induced martensitic transformation, the medium SFE favors deformation twinning [3]. Other than the SFE, crystallographic orientation and grain size affect the deformation twinning behavior of TWIP steels. Deformation twinning mainly occurred in grains oriented close to the ⟨111⟩ // tensile axis where the maximum resolved shear stress for twinning is larger than that for the slip, while only a small portion of the grains oriented close to the ⟨100⟩ // tensile axis exhibited deformation twinning [1,4]. The fraction of DTs was reported to be higher with increasing grain size of the TWIP steel [5]. The twin nucleation stress was reported to increase with decreasing grain size, and the primary DTs were thinner in the fine grain material than in the coarse grain material [6].

To investigate deformation mechanisms of TWIP steels, advanced microstructural analysis techniques such as synchrotron X-ray diffraction (XRD) [7], electron backscattering diffraction (EBSD) [8], electron channeling contrast imaging (ECCI) [9], 3D atom probe tomography (3D-APT) [10], and transmission electron microscopy (TEM) [3] have been utilized. Further, the microstructure-mechanical properties relationship has been investigated in terms of temperature/strain rate-dependent mechanical properties [11,12] and micromechanical constitutive modeling considering microstructure evolution upon deformation [13,14]. However, detailed dynamics of deformation mechanisms are hardly identified using conventional analyses. Thus, in-situ characterization techniques upon deformation are required such as in-situ synchrotron X-ray diffraction, SEM, EBSD, and TEM.

In this regard, in-situ TEM mechanical testing is an efficient tool to provide direct insights into fundamental deformation mechanisms of materials [15]. Several previous works are available on in-situ TEM

E-mail address: jinkyungkim@hanyang.ac.kr.

https://doi.org/10.1016/j.matchar.2022.112583
Received 3 June 2022; Received in revised form 23 September 2022; Accepted 10 December 2022
Available online 12 December 2022

mechanical testing of TWIP steels [16–18]. Kim et al. [17] reported the formation of a thin twin by Shockley partial dislocations emitted from a grain boundary, which indicates the nucleation of DTs at grain boundary defect sites. The reported twinning process is similar to DT in nanocrystalline materials through successive emission of partial dislocations from grain boundaries. Fu et al. [18] reported governing role of dislocation activity on the plasticity of the TWIP steel by observing planar slip and cross-slip of dislocations from in situ TEM mechanical testing.

However, to unravel the deformation mechanisms of TWIP steels, more key observations by in-situ TEM mechanical testing are required. Therefore, the present work reports three deformation mechanisms of TWIP steels observed by in-situ TEM mechanical testing. (1) DTs were nucleated from grain boundaries, which confirms the universality of the phenomenon in TWIP steels [17]. (2) Growth of a deformation twin was blocked by a stacking fault (SF). While SFs have been reported to contribute to strain hardening of FCC materials [19], direct observationsof stacking faults blocking the motion of defects are hardly available from early works. (3) Motion of extended dislocations contributing to the plasticity of the material was observed. While extended dislocations consisting of two Shockley partial dislocations are widely observed in the low SFE FCC materials [20], their dynamic motion contributing to the plasticity of the material is a novel observation.

2. Experimental

The Fe-16.6Mn-0.45C-1.57Al-1Si-0.062Ti-0.007 N (wt%) TWIP steel was used for the present work. The ingots were homogenized at 1180 °C for 1 h and hot-rolled to a thickness of 2.5 mm. Since the as-hot rolled steel was not fully recrystallized, annealing at 1000 °C for 10 min was conducted to achieve the fully recrystallized microstructure. The EBSD transverse direction (TD) inverse pole figure (IPF) map of the annealed material (Fig. 1) shows a fully-recrystallized microstructure with an average grain size of 11.6 μm and random grain orientation. The in-situ TEM observations were conducted following the procedure reported in the previous work [17]. TEM samples for in-situ TEM straining tests were prepared as 3 mm diameter discs which were mechanically polished to a thickness less than 100 μm and thinned by twin-jet electropolishing at room temperature. A mixture of 5% perchloric acid and 95% acetic acid was used as an electrolyte. The edges of the 3 mm diameter disks were trimmed to have a width of 1.8 mm to obtain the samples elongated along the tensile direction. The disk was glued on a rectangular Cu support, and loaded on a singled tilt, straining TEM holder (Model 652TM, Gatan) which elongated the sample via a micrometer screw driven by a DC motor.

3. Results and discussion

3.1. Formation of deformation twins from grain boundaries

The snapshots of an in-situ TEM straining test (Fig. 2, Movie S1) provide evidence of the formation of DTs by direct emission of Shockley partial dislocations from grain boundary sources [17]. Two overlapped planar defects with the fringe contrast, indicated by labels 1 and 2, are present near the grain boundary (Fig. 2(a)). Fig. 2(b) shows that the contrast of the lower part of the planar defect 1 changes from the fringe contrast to the white contrast by the motion of dislocation A. As deformation proceeds, the contrast of the upper part of the planar defect also changes from the fringe contrast to the white contrast by the motion of dislocation B (Fig. 2(d)). The contrast change from the fringe to white corresponds to the formation of a thin twin with the thickness of multiple of three atomic layers by the movement of a single twinning partial dislocation [17]. Thus, dislocations A and B are most likely twinning partial dislocations. Further deformation leads to the further motion of dislocation B while dislocation A does not move much (Fig. 2(e)). This indicates a quite different degree of growth kinetics of DTs depending upon local stress states.

3.2. Interactions between a deformation twin and a stacking fault

Snapshots of another in-situ TEM straining test show interactions of the planar defects on different {111} planes (Fig. 3, Movie S2). The four parallel planar defects as seen edge-on from the viewing direction of TEM are indicated by the labels 1, 2, 3, and 4. The two inclined planar defects showing a fringe contrast are indicated by labels 5 and 6. The particle indicated by the white arrow corresponds to the (Fe, Mn)C carbide. Note that planar defect 5 is confined between the carbide and planar defect 1. Planar defect 5 was most likely emitted from the carbide since a particle in the matrix could act as a location of local stress concentration [21]. Planar defect 5 shows mixed fringe and white contrast inside the plate. The white fault was identified as a thin twin with the thickness of multiple of three atomic layers because the SF contrast vanishes for every third stacking fault [17]. Therefore, planar defect 5 is most likely an inclined DT. Inside planar defect 5, the main visible dislocations are indicated by the labels A, B, C, and D. Dislocations A and B near planar defect 1 are almost stationary while dislocations C and D move towards the planar defect 1 as deformation proceeds.

To identify the phenomena occurring at the interfaces of planar defect 1, TEM images were recorded near planar defect 1 during the in-situ straining test. Note that the same labels as Fig. 3 were used in Fig. 4. Fig. 4(a) shows the same microstructural features shown in Fig. 3. Dislocation A shows the narrow SF contrast, which indicates closely present two Shockley partial dislocations. Dislocations B, C, and D are trailing the fault having the fringe contrast or white contrast, showing

Fig. 1. The EBSD transverse direction (TD) inverse pole figure (IPF) map of the annealed material, showing a fully-recrystallized microstructure with an average grain size of 11.6 μm and random grain orientation.

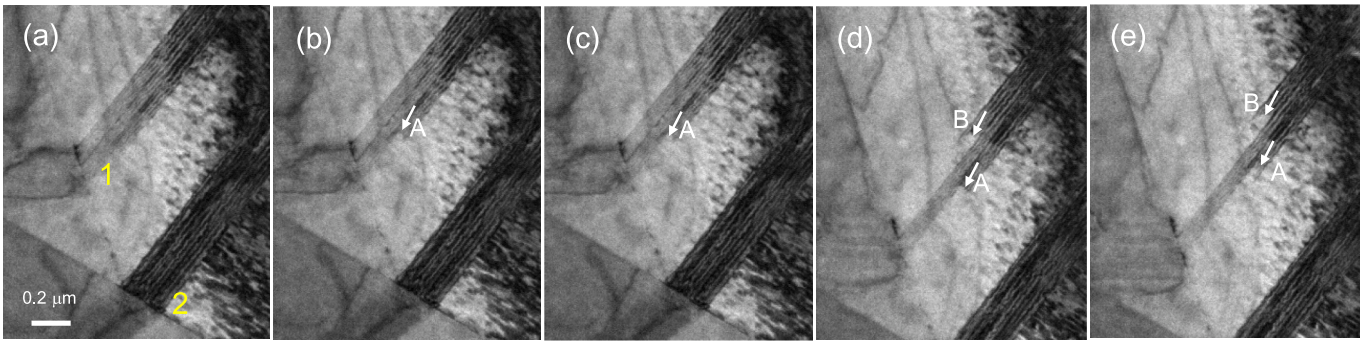

Fig. 2. The snapshots of an in situ TEM straining test providing evidence of the formation of DTs by direct emission of Shockley partial dislocations from grain boundary sources. (a) Two overlapped planar defects with the fringe contrast, indicated by labels 1 and 2 near the grain boundary. (b) The contrast change of the lower part of planar defect 1 from the fringe contrast to the white contrast by the motion of dislocation A. (c) Further motion of dislocation A trailing the white contrast fault. (d) The contrast change of the upper part of the planar defect from the fringe contrast to the white contrast by the motion of dislocation B. (e) The further motion of dislocation B and almost stationary dislocation A.

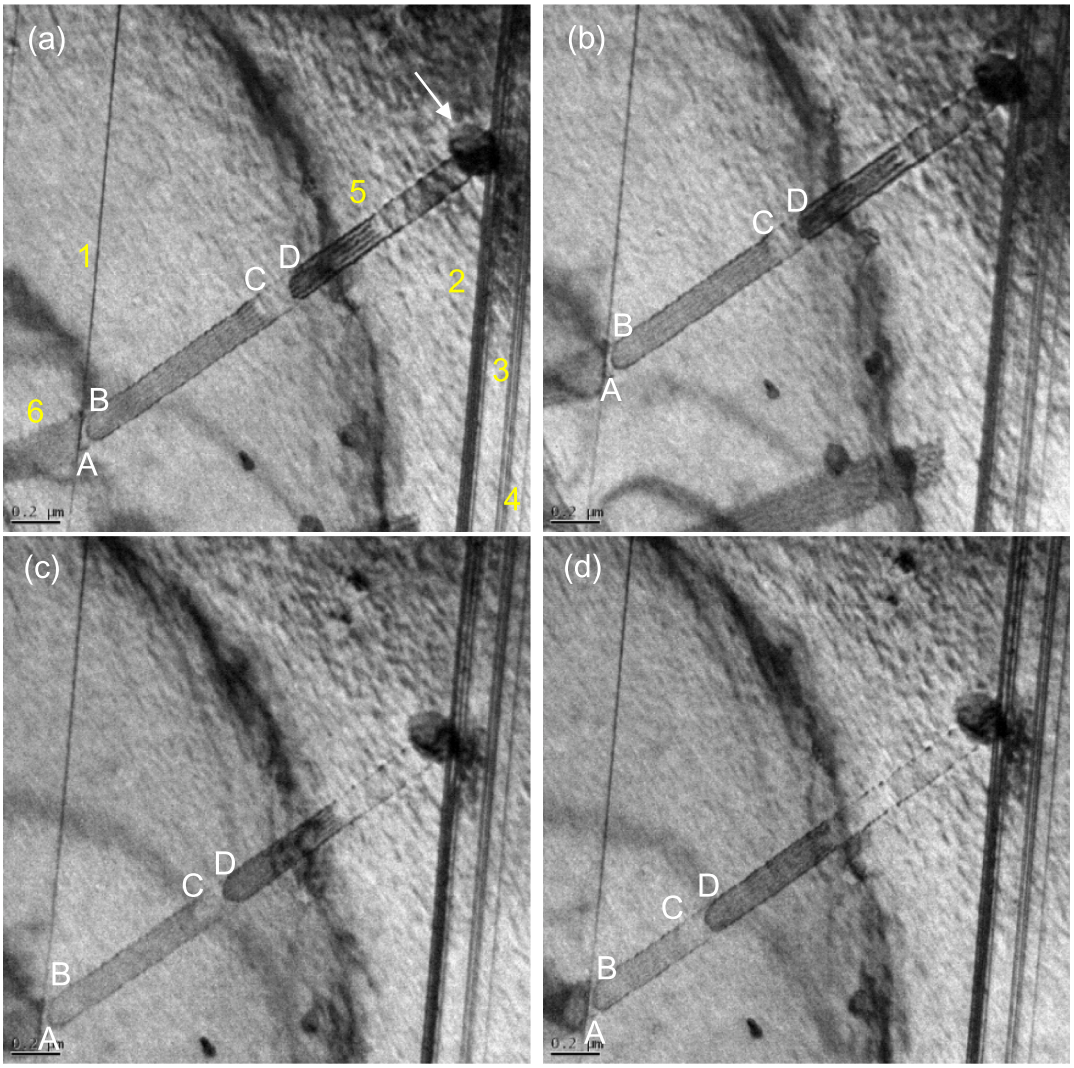

Fig. 3. Snapshots of an in situ TEM straining test showing interactions of the planar defects on different {111} planes. The four parallel planar defects as seen edge-on from the viewing direction of TEM are indicated by labels 1, 2, 3, and 4. The two inclined planar defects showing a fringe contrast are indicated by labels 5 and 6. The particle indicated by the white arrow corresponds to the (Fe, Mn)C carbide. Planar defect 5 is an inclined twin confined between the carbide and planar defect 1. (a) Inside planar defect 5, the main visible dislocations are indicated by labels A, B, C, and D. (b)-(d) Dislocations A and B near planar defect 1 are almost stationary while dislocations C and D move towards planar defect 1 as deformation proceeds.

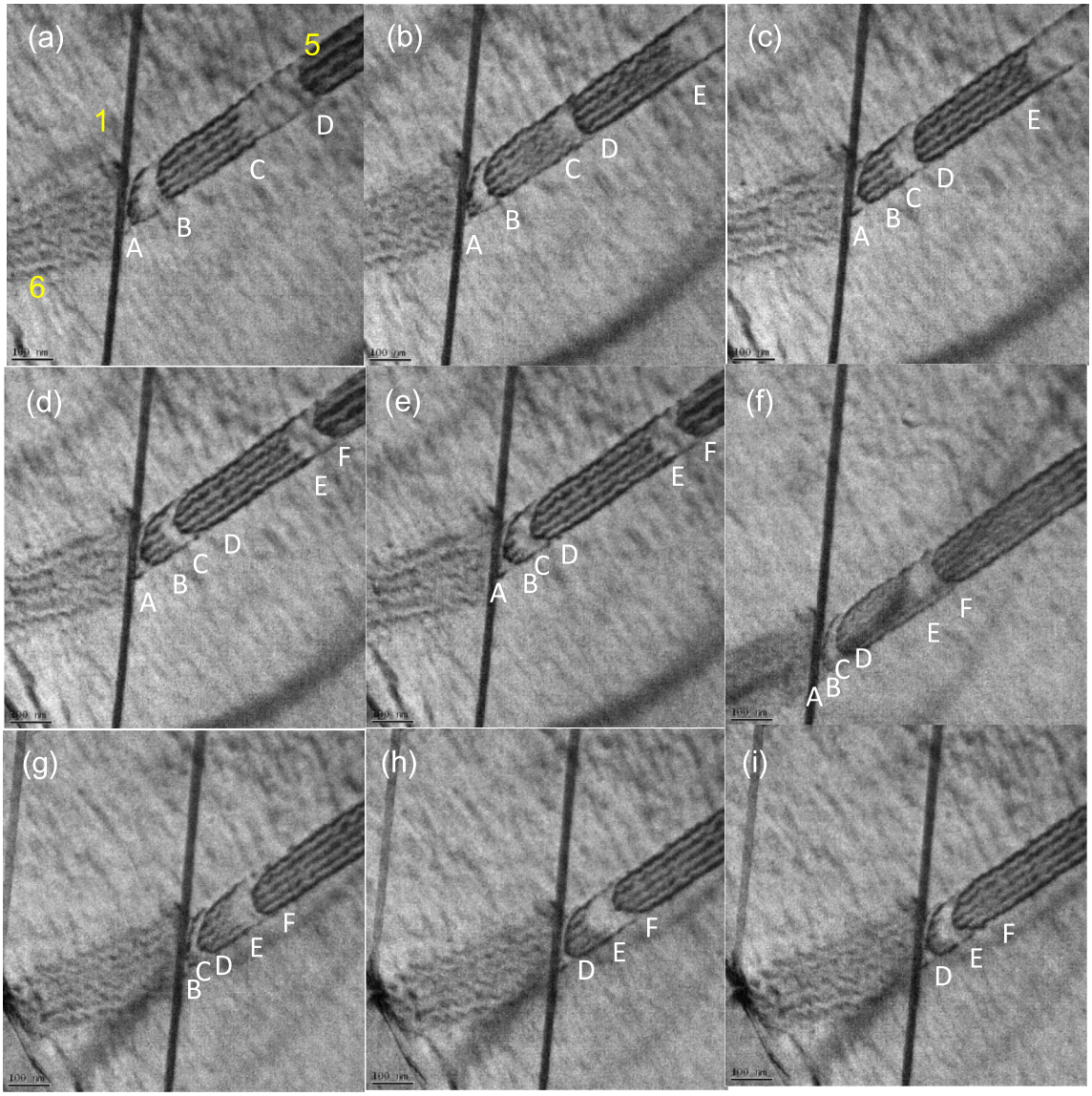

Fig. 4. Snapshots recorded near planar defect 1 from the in-situ TEM straining test shown in Fig. 3. The same labels as Fig. 3 were used. Dislocations A to F are visible in the planar defect 5. (a) Dislocation A shows the narrow SF contrast, which indicates closely present two Shockley partial dislocations. Dislocations B, C, and D are trailing the fault having the fringe contrast or white contrast, indicating their characteristics of Shockley partial dislocations. (b) Dislocation B approaches dislocation A while dislocation D approaches dislocation C. The dislocation E trailing the fault with the white contrast is visible. (c) Dislocation A approaches the interface of planar defect 1 so that the contrast of an extended dislocation is not visible. The distance between dislocation B and dislocation C becomes smaller compared to the snapshot in (b). (d) A newly identified dislocation F trailing the fault with the fringe contrast. (e) Dislocation B and dislocation C are closely present, leading to the narrow SF contrast. (f) The close presence of dislocations A, B, C, and D due to the motion of the dislocations and the approach of dislocations E and F towards planar defect 1. (g) The contrast of dislocation A is not visible, indicating the absorption of the dislocation due to its interaction with the planar defect 1. (h) The contrast of dislocations B and C is not visible. (i) The close presence of dislocations D and E leads to the narrow SF contrast.

characteristics of Shockley partial dislocations. In Fig. 4(b), dislocation B approaches dislocation A while dislocation D approaches dislocation C. The dislocation E trailing the fault with the white contrast is also visible. Fig. 4(c) shows that dislocation A approached closely the interface of planar defect 1 so that the contrast of an extended dislocation is not visible. The distance between dislocation B and dislocation C becomes smaller compared to the snapshot in Fig. 4(b). Fig. 4(d) shows a newly identified dislocation F trailing the fault with the fringe contrast. In Fig. 4(e), dislocation B and dislocation C are closely present, leading to the narrow SF contrast. Fig. 4(f) shows the close presence of dislocations A, B, C, and D due to the motion of the dislocations and the approach of dislocations E and F towards planar defect 1. In Fig. 4(g), the contrast of dislocation A is not visible, indicating the absorption of the dislocation due to its interaction with the planar defect 1. In Fig. 4 (h), the contrast of dislocations B and C is not visible. In Fig. 4(i), the close presence of dislocations D and E leads to the narrow SF contrast.

To characterize the defects observed in the in-situ straining TEM test, postmortem TEM analysis was conducted at the same location. Fig. 5 shows two-beam TEM BF images showing the same region presented in Figs. 3 and 4. Note that the same labels as Figs. 3 and 4 were used in Fig. 5, and planar defects 1 to 6 could be identified. The micrograph was mirrored due to the change in sample orientation during the reloading of the TEM specimen. When compared to the [110] zone axis diffraction pattern, planar defects 1 to 4 are parallel to the $(\bar{1}11)$ plane of the FCC matrix. The thickness of planar defects 1, 2, 3, and 4 are 52 nm, 100 nm, 90 nm, and 70 nm, respectively. The dark contrast of planar defects 2 and 3 suggests that they are most likely DTs with a high density of defects inside the plates. However, the zone axis diffraction pattern taken

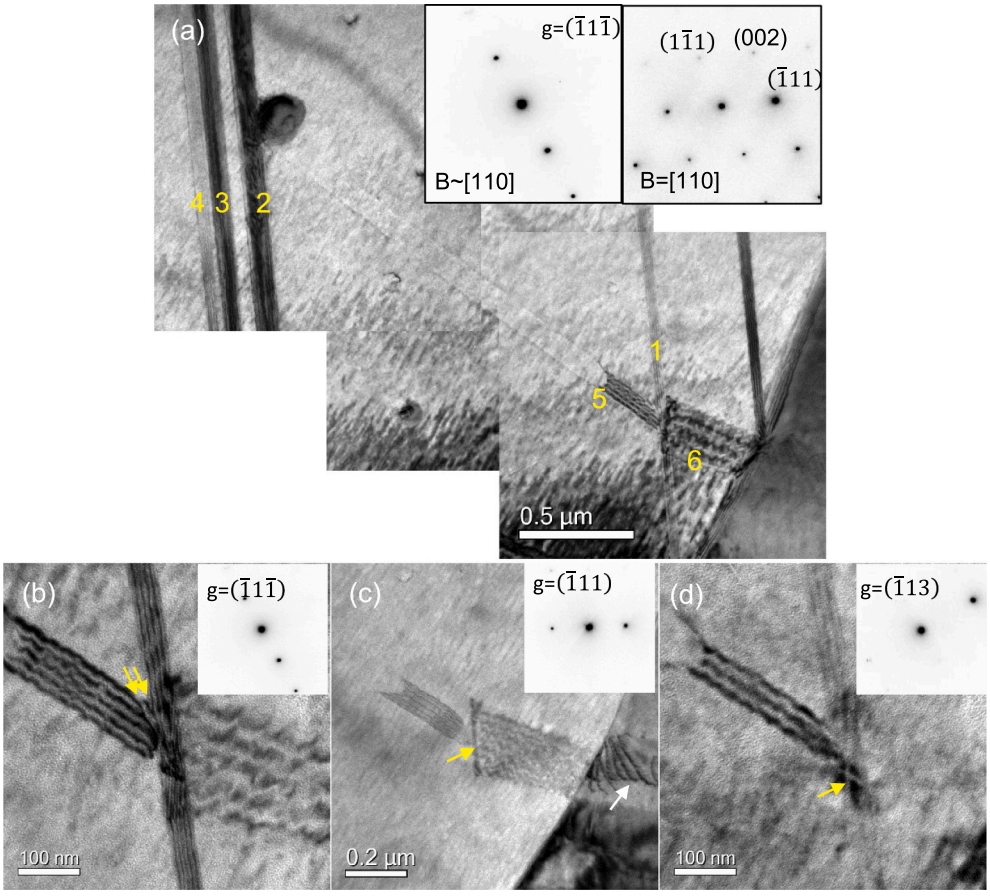

Fig. 5. Postmortem two-beam TEM BF images obtained from the same location observed from the in-situ TEM straining test shown in Figs. 2 and 3. The same labels as Figs. 2 and 3 were used in Fig. 4. The micrograph was mirrored due to the change in sample orientation during the reloading of the TEM specimen. (a) Planar defects 2 and 3 with the dark contrast are most likely DTs with a high density of defects inside the plates while planar defect 1 corresponds to a SF. (b)-(d) Two-beam diffraction analysis using several diffraction conditions conducted at the junction where planar defects 1, 5, and 6 are overlapped.

on planar defect 1 did not reveal the presence of spots from DTs. This suggests that planar defect 1 corresponds to a SF. Therefore, the observed phenomena in Fig. 4 correspond to interactions between a DT (planar defect 5) and a SF (planar defect 1). To identify the dislocations present in the planar defects, a two-beam diffraction analysis using several diffraction conditions was conducted. The analysis was conducted at the junction where planar defects 1, 5, and 6 are overlapped. The two-beam BF image taken with g=$(\bar{1}1\bar{1})$ (Fig. 5(b)) shows the contrast of two dislocations as indicated by the yellow arrows. For this two-beam condition, perfect dislocation with the Burgers vector of $\frac{1}{2}[0\bar{1}1]$ or $\frac{1}{2}[1\bar{1}0]$ and Shockley partial dislocation with the Burgers vector of $\frac{1}{6}[1\bar{2}1]$ can be visible. Because the two dislocations are bound to planar defect 5, the two dislocations are most likely Shockley partial dislocations with the same Burgers vector. The two-beam BF image taken with g=$(\bar{1}11)$ (Fig. 5(c)) shows that planar defect 1 is out of contrast from the $g{\cdot}R = 0$ criterion. For this two-beam condition, the contrast of dislocation bounding planar defect 6 is only visible as indicated by the yellow arrow. Note that some dislocations are present in the neighboring grain as indicated by the white arrow. The dislocations could act as stress-relaxation mechanisms for the highly localized stress at the grain boundary [17]. The two-beam BF image taken with g=$(\bar{1}13)$ (Fig. 5(d)) shows a dislocation contrast that seems to be related to planar defect 1. For this two-beam condition, various types of dislocations such as perfect, Shockley partial, and Frank partial dislocations can be visible. However, the two-beam condition makes the Shockley partial dislocation with the Burgers vector of $\frac{1}{6}[1\bar{2}1]$ invisible, indicating that the dislocation contrast in Fig. 5(d) is different from that in Fig. 5(b).

The present work reports the initial stage deformation behavior of TWIP steel. Nucleation of DTs was observed at the grain boundary (Fig. 2) and near the precipitate and a twin boundary (Fig. 3). Both locations can be considered as regions with stress concentration, where DTs can be easily nucleated to relax the localized stress. In the inclined twin shown in Fig. 3, the motion of Shockley partial dislocations was observed, thereby leading to the growth of the DT. Fig. 4 shows the disappearance of Shockley partial dislocations near the SF. Wei et al. [22] proposed from molecular dynamics (MD) simulations the three types of interactions between a screw dislocation and a SF in FCC metals: (1) dissociation of a lattice dislocation into two Shockley partial dislocation on an adjacent plane parallel to SF, leading to the thickening of the SF, (2) the same dissociation, but propagating of the two Shockley partial dislocations oppositely along the SF plane, leading to the annihilation of the SF, and (3) penetration of the lattice dislocation and dissociation into an extended dislocation on the other side of the SF. The present observation is different from the simulation because the incoming dislocations are not perfect dislocations, but Shockley partial dislocations. Among the three types of interactions, interaction (2) is not likely to occur because the SF is present after the interactions with dislocations. The evidence of dislocation penetration suggested for interaction (3) was not obtained. Therefore, the observed interaction in the in-situ TEM experiment could correspond to interaction (1). Interaction (1) requires recombination of the two Shockley partial dislocations into a perfect dislocation, cross-slip of the dislocation onto the SF plane, and dissociation into two Shockley partial dislocations on the SF plane.

The motion of Shockley partial dislocations A and B in the twin is blocked by the SF while dislocations C and D far from the SF relatively freely move (Fig. 3). The observed sluggish motion of Shockley partial dislocations (Figs. 3–5) near the SF suggests a strengthening effect of SFs. Wei et al. [22] showed by molecular dynamics (MD) simulation that leading partial dislocations are generally blocked by the stacking fault until recombination of the leading and the trailing partial dislocations

occurs under sufficient external stress. They further suggested that the stress necessary for the dislocation to cross slip along the SF or penetrate through the SF is higher than the critical resolved shear stress for the recombination of partial dislocations, leading to the strengthening effect of the SF [22,23].

3.3. Direct observation of extended dislocations plasticity

Snapshots of another in-situ TEM straining test (Movie S3) show direct evidence of the motion of extended dislocations. In Fig. 6(a), the four parallel planar defects are indicated by the labels 1, 2, 3, and 4. As deformation proceeds, the motion of dislocations on different slip planes, i.e. the dislocation indicated by the yellow arrow and the white arrow, is observed. To characterize the phenomena occurred during the in-situ TEM straining test, postmortem TEM analysis was conducted at the same location. The micrograph was mirrored due to the change in sample orientation during the reloading of the TEM specimen. Planar defect 1 shows a high density of Shockley partial dislocations inside the plate. Planar defect 2 shows the mixed fringe and white contrast while planar defects 3 and 4 show only fringe contrast. The three dislocations showing the narrow fringe contrast, located between planar defects 3 and 4, are indicated by the labels A, B, and C. The narrow fringe contrast indicates that the three dislocations are extended dislocations. In Fig. 6 (a), dislocations A, B, and C are visible and they are trailing slip traces present on the TEM specimen surface formed by the movement of the extended dislocations. The dislocation indicated by the white arrow shows the same contrast as dislocations A, B, and C, which suggests the nature of an extended dislocation. The dislocation indicated by the yellow arrow is present inside planar defect 2 and thus corresponds to a Shockley partial dislocation inside the DT with the white contrast.

Fig. 6 shows direct evidence of motion of extended dislocation across the entire grain. This suggests a contribution of extended dislocation slip on the plasticity of TWIP steels. Fu et al. [18] reported significant activation of cross-slip and dislocation interactions in the in-situ TEM observations of the Fe-30Mn-3Si-3Al (wt%) TWIP steel, which also suggests a major role of dislocation slip on accommodation of plastic strain.

4. Conclusions

The present work reports three deformation mechanisms of TWIP steels observed by in-situ TEM mechanical testing: (1) formation of deformation twins from gran boundaries, (2) interference of growth of DTs by SF, and (3) motion of extended dislocations contributing to the plasticity.

(1) Formation of DTs by direct emission of Shockley partial dislocations from grain boundary sources was observed. The different degree of the motion of twinning partial dislocations indicates a different degree of growth kinetics of DTs depending upon local stress states.
(2) Nucleation of DTs was observed near the precipitate and a twin boundary. Shockley partial dislocations moved in the inclined twin, leading to the growth of the DT. The sluggish motion of Shockley partial dislocations near the SF suggests a strengthening effect of SFs.

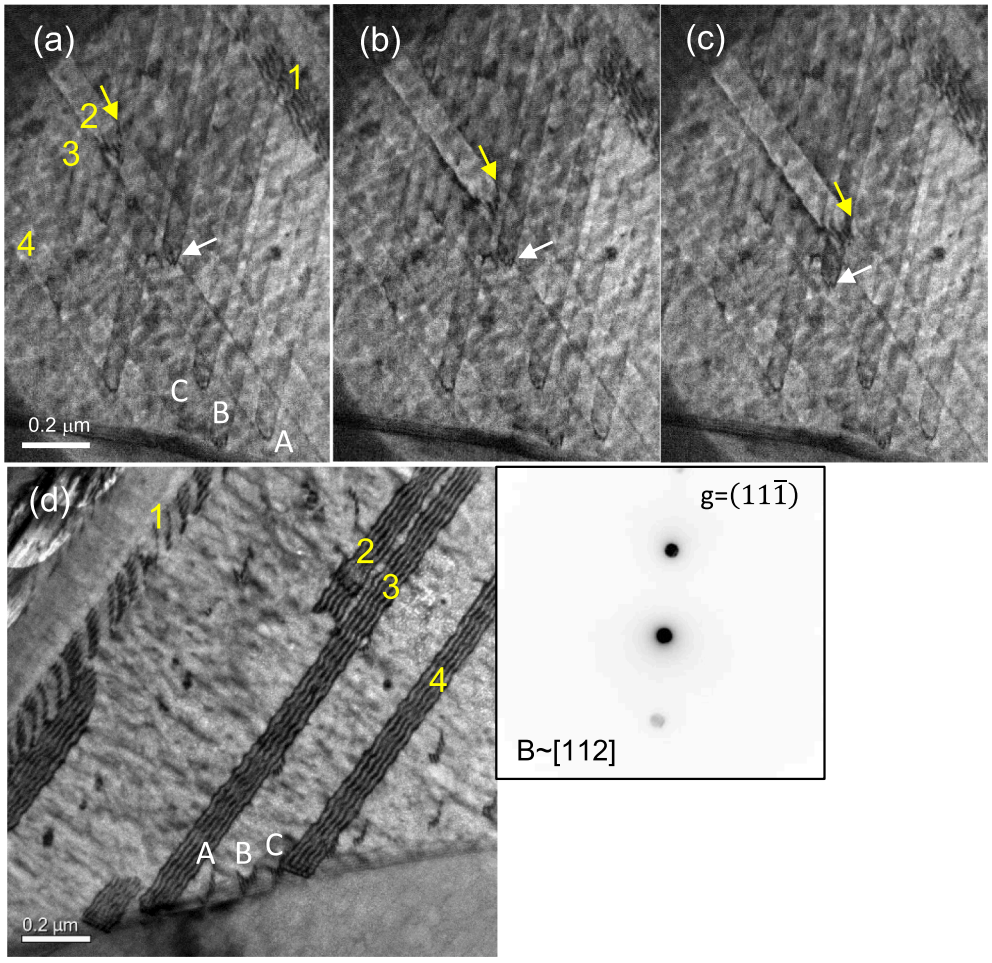

Fig. 6. (a)-(c) Snapshots of an in situ TEM straining test showing direct evidence of the motion of extended dislocations. The four parallel planar defects are indicated by labels 1, 2, 3, and 4. As deformation proceeds, the motion of dislocations on different slip planes, i.e. the dislocation indicated by the yellow arrow and the white arrow, is observed. (d) Postmortem two-beam TEM BF image obtained from the same location. The micrograph was mirrored due to the change in sample orientation during the reloading of the TEM specimen. Dislocations A, B, and C with the narrow fringe contrast, located between planar defects 3 and 4, correspond to extended dislocations. The dislocation indicated by the yellow arrow and the white arrow shown in (a)-(c) corresponds to a Shockley partial dislocation inside the DT and an extended dislocation, respectively. (For interpretation of the references to colour in this figure legend, the reader is referred to the web version of this article.)

(3) Direct evidence of motion of extended dislocation across the entire grain was obtained, which suggests a contribution of extended dislocation slip on the plasticity of TWIP steels.

Supplementary data to this article can be found online at https://doi.org/10.1016/j.matchar.2022.112583.

Declaration of Competing Interest

The authors declare that they have no known competing financial interests or personal relationships that could have appeared to influence the work reported in this paper.

Data availability

The raw/processed data required to reproduce these findings cannot be shared at this time due to technical or time limitations.

Acknowledgement

This research was supported by the Basic Science Research Program through the National Research Foundation of Korea funded by the Ministry of Education (2018R1D1A1B07044731), NRF-2021R1F1A1046001.

References

[1] B.C. De Cooman, Y. Estrin, S.K. Kim, Twinning-induced plasticity (TWIP) steels, Acta Mater. 142 (2018) 283–362.
[2] J. Kim, Y. Estrin, B.C. De Cooman, Application of a dislocation density-based constitutive model to Al-alloyed TWIP steel, Metall. Mater. Trans. A 44 (9) (2013) 4168–4182.
[3] J.K. Kim, B.C. De Cooman, Stacking fault energy and deformation mechanisms in Fe-xMn-0.6C-yAl TWIP steel, Mater. Sci. Eng. A 676 (2016) 216–231.
[4] I. Gutierrez-Urrutia, S. Zaefferer, D. Raabe, The effect of grain size and grain orientation on deformation twinning in a Fe–22wt.% Mn–0.6wt.% C TWIP steel, Mater. Sci. Eng. A 527 (15) (2010) 3552–3560.
[5] H. Gwon, J.H. Kim, J.-K. Kim, D.-W. Suh, S.-J. Kim, Role of grain size on deformation microstructures and stretch-flangeability of TWIP steel, Mater. Sci. Eng. A 773 (2020), 138861.
[6] K.M. Rahman, V.A. Vorontsov, D. Dye, The effect of grain size on the twin initiation stress in a TWIP steel, Acta Mater. 89 (2015) 247–257.
[7] K. Yan, D.G. Carr, M.D. Callaghan, K.-D. Liss, H. Li, Deformation mechanisms of twinning-induced plasticity steels: in situ synchrotron characterization and modeling, Scr. Mater. 62 (5) (2010) 246–249.
[8] D. Barbier, N. Gey, S. Allain, N. Bozzolo, M. Humbert, Analysis of the tensile behavior of a TWIP steel based on the texture and microstructure evolutions, Mater. Sci. Eng. A 500 (1–2) (2009) 196–206.
[9] I. Gutierrez-Urrutia, D. Raabe, Dislocation and twin substructure evolution during strain hardening of an Fe–22wt.% Mn–0.6wt.% C TWIP steel observed by electron channeling contrast imaging, Acta Mater. 59 (16) (2011) 6449–6462.
[10] M. Herbig, M. Kuzmina, C. Haase, R.K.W. Marceau, I. Gutierrez-Urrutia, D. Haley, D.A. Molodov, P. Choi, D. Raabe, Grain boundary segregation in Fe-Mn-C twinning-induced plasticity steels studied by correlative electron backscatter diffraction and atom probe tomography, Acta Mater. 83 (2015) 37–47.
[11] M. Madivala, A. Schwedt, S.L. Wong, F. Roters, U. Prahl, W. Bleck, Temperature dependent strain hardening and fracture behavior of TWIP steel, Int. J. Plast. 104 (2018) 80–103.
[12] M. Madivala, A. Schwedt, U. Prahl, W. Bleck, Anisotropy and strain rate effects on the failure behavior of TWIP steel: a multiscale experimental study, Int. J. Plast. 115 (2019) 178–199.
[13] D.R. Steinmetz, T. Jäpel, B. Wietbrock, P. Eisenlohr, I. Gutierrez-Urrutia, A. Saeed-Akbari, T. Hickel, F. Roters, D. Raabe, Revealing the strain-hardening behavior of twinning-induced plasticity steels: theory, simulations, experiments, Acta Mater. 61 (2) (2013) 494–510.
[14] J.K. Kim, Y. Estrin, B.C. De Cooman, Constitutive modeling of the stacking fault energy-dependent deformation behavior of Fe-Mn-C-(Al) TWIP steels, Metal. Mater. Trans. A Phys. Metal. Mate. Sci. 49 (12) (2018) 5919–5924.
[15] E. Spiecker, S.H. Oh, Z.-W. Shan, Y. Ikuhara, S.X. Mao, Insights into fundamental deformation processes from advanced in situ transmission electron microscopy, MRS Bull. 44 (06) (2019) 443–449.
[16] S.-I. Baik, T.-Y. Ahn, W.-P. Hong, Y.-S. Jung, Y.-K. Lee, Y.-W. Kim, In situ observations of transgranular crack propagation in high-manganese steel, Scr. Mater. 100 (2015) 32–35.
[17] J.-K. Kim, M.-H. Kwon, B.C. De Cooman, On the deformation twinning mechanisms in twinning-induced plasticity steel, Acta Mater. 141 (2017) 444–455.
[18] X. Fu, X. Wu, Q. Yu, Dislocation plasticity reigns in a traditional twinning-induced plasticity steel by in situ observation, Mater. Today Nano 3 (2018) 48–53.
[19] Y.Z. Tian, L.J. Zhao, S. Chen, A. Shibata, Z.F. Zhang, N. Tsuji, Significant contribution of stacking faults to the strain hardening behavior of Cu-15%Al alloy with different grain sizes, Sci. Rep. 5 (1) (2015) 16707.
[20] J.-K. Kim, J.H. Kim, H. Park, J.-S. Kim, G. Yang, R. Kim, T. Song, D.-W. Suh, J. Kim, Temperature-dependent universal dislocation structures and transition of plasticity enhancing mechanisms of the Fe40Mn40Co10Cr10 high entropy alloy, Int. J. Plast. 148 (2022), 103148.
[21] D. You, G. Yang, Y.-H. Choa, J.-K. Kim, Crack-resistant σ/FCC interfaces in the Fe40Mn40Co10Cr10 high entropy alloy with the dispersed σ-phase, Mater. Sci. Eng. A 831 (2022), 142039.
[22] H. Wei, Y. Wei, Interaction between a screw dislocation and stacking faults in FCC metals, Mater. Sci. Eng. A 541 (2012) 38–44.
[23] R. Su, D. Neffati, Y. Zhang, J. Cho, J. Li, H. Wang, Y. Kulkarni, X. Zhang, The influence of stacking faults on mechanical behavior of advanced materials, Mater. Sci. Eng. A 803 (2021).